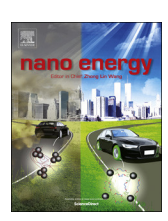
ELSEVIER

Contents lists available at ScienceDirect

Nano Energy

journal homepage: www.elsevier.com/locate/nanoen



Full paper

Polarization effects of transition dipoles on photoluminescence and photocurrent in organic-inorganic hybrid perovskites



Shengbo Ma, Hengxing Xu, Miaosheng Wang, Jiajun Qin, Ting Wu, Ping Chen, Bin Hu

Department of Materials Science and Engineering, University of Tennessee, Knoxville, TN, 37996, USA

ARTICLE INFO

Keywords:
Organic-inorganic hybrid perovskites
Photo-induced polarization
Photoluminescence
Photocurrent
Transition dipole moment

ABSTRACT

Polarization effects on optoelectronic behaviors in perovskite-based devices are difficult to address due to quick electronic polarization relaxation and ionic polarization from mobile ions. Here we show the effects of polarized excited states on photoluminescence and photocurrent in MAPbBr₃ thin-film devices. We found optically polarized transition dipoles, oriented paralleled and perpendicular to device built-in field, give rise to significantly different photoluminescence and photocurrent outcomes. It provides a new understanding that controlling domain geometry can further enhance the light-emitting and photovoltaic performance of perovskite-based applications. The observation proves that the anisotropy of photoexcited transition dipoles is existed in the electronic states of MAPbBr3. Particularly, this indicates that photo-induced electronic polarization can be shown as photoinduced dielectric polarization at the dipolar polarization regime, which impacts device performance. We also observed that increasing photoexcitation intensity leads to a decreases on both field-induced photoluminescence quenching and field-induced photocurrent enhancing, which implies a cooperative interaction between transition dipoles of increased density that favors light emission but infavors charge dissociation. This provides a critical understanding on why organic-inorganic hybrid perovskites can function as efficient photovoltaic and light-emitting materials at low and high excitation intensities, respectively. Our estimation shows that, by manipulating the ratio of dipole orientation, the efficiencies of perovskite-based LEDs and solar cells could be improved by 50% and 18%, respectively. Clearly, the polarization effect presents a new insight on further controlling photovoltaic and light-emitting actions by manipulating the polarization of excited states in perovskite optoelectronics.

1. Introduction

The organic-inorganic hybrid perovskites (OIHPs) have emerged as one of the most promising materials for highly efficient photovoltaics (PV) [1–4]. Besides, this class of materials have been found as multifunctional materials for different applications including photodetectors [5], light-emitting device (LED) [6–8], lasing [9–11], and field-effect transistors [12–14]. More interestingly, it was shown that OIHPs are electrically and optically polarizable [15–19]. The polarization is reported caused by field-induced ion/defect migration [20,21], ferroelectric properties due to the rotational freedom of the dipolar organic cations (such as MA⁺) [22–25], and large polaron formation due to the deformation of the inorganic sublattice ([PbX₃]) [26,27]. The photo-induced polarization, associated with fundamental photophysical behaviors, significantly impacts the performance of optoelectronic applications and requires more efforts. Several studies have shown that photo-induced polarization plays an important role in determining

photovoltaic actions in inorganic ferroelectric materials [28,29]. For example, the horizontally oriented in-plane component of the ferroelectric polarization generated maximum photocurrent in BiFeO3 single-domain crystals when excited by polarized light with parallel polarization [30]. In OIHP thin films, the in-plane and out-of-plane transition dipole moments were observed, which were excited by linearly polarized photoexcitation perpendicular and parallel to the incident plane, respectively [31]. Furthermore, it was revealed that in MAPbI₃ thin film the excited states induced by polarized photoexcitation maintain a polarization memory (~150 ps) which leads to a transient polarized photoluminescence (PL) emission at room temperature [17,18]. Recently, it has been reported that polarization memory was also observed in MAPbBr₃ films [32]. The study indicated that the intrinsic transition dipole moments, depending on both light polarization and polar distortion of local crystal lattice, is responsible for the polarization memory. A significant polarization loss has also been reported when utilizing above-bandgap photoexcitation in the

^{*} Corresponding author.

E-mail address: bhu@utk.edu (B. Hu).

study, which implies the difficulty to investigate the polarization effects on steady-state optoelectronic behaviors in perovskite-based devices. The published works on transition dipole moments and polarization memories have proved the existence of polarized excited states and their picosecond-timescale relaxation lifetime in OIHPs. Orientation of the transition dipole moments has been known as a critical factor influencing device efficiencies in optoelectronic applications [33,34]. Therefore, it can be expected that manipulating photo-induced polarization in OIHPs can provide a new approach to influence the device performance. However, photo-induced polarization in OIHPs is occurred at the electronic regime (~1015 Hz). Normally, such high-frequency polarization can negligibly impact the steady-state device performance controlled by dielectric polarization at low frequency $(< 10^6 \, \mathrm{Hz})$. In our work, we demonstrate that it is possible to convert the transient polarization from electronic polarization regime to dipolar polarization regime (~106 Hz), found by manipulating their orientdependent dissociation under device-operating condition, and consequently improves the performance of OIHP based LEDs and solar cells. We also reveal that the mechanism responsible for dissociation of transition dipoles is dependent on their orientation in internal electric field under device-operating condition, which will consequently lead to polarization effect of steady-state photoluminescence and photocurrent. It opens new opportunities to further improve the light-emitting and photovoltaic performance by manipulating the polarization of excited states in OIHP optoelectronic devices through controlling domain geometry.

In this work, we investigate the polarization effect of transition dipoles on photoluminescence and photocurrent in OIHP thin-film devices by utilizing linearly polarized photoexcitation with distinct orientations under device-operating conditions at room temperature. In our studies, the p- and s- polarized photoexcitation is provided by linearly polarized 405-nm laser, generating the p- and s- polarized transition dipoles in OIHP layer, respectively. The p-polarized transition dipoles are vertical-oriented, parallel to the built-in field, while the spolarized transition dipoles are horizontally-oriented, perpendicular to the built-in field. A negative bias is then applied to the device to enhance the built-in field, which facilitates the charge dissociation of excited states and consequently suppresses the radiative recombination. It is observed that horizontally and vertically polarized transition dipoles lead to distinct bias-dependent photoluminescence and photocurrent curves under identical excitation intensity, of which the first derivatives reflect the field-induced dissociation enhancement. We found vertically p-polarized transition dipoles encounter larger charge dissociation compared to horizontally s-polarized transition dipoles under identical electric field, which is implied consistently by both biasdependent PL and photocurrent measurements. The distinct dissociation rates indicate that transition dipoles can maintain their photo-induced polarization in MAPbBr3 film until they are dissociated into free charge carriers, and the dissociation is dependent on the polarization orientation with respect to the internal electric field. Moreover, it is also observed that the field-induced PL quenching is decreased when increasing photoexcitation intensity for both p- and s- polarized photoexcitation. This observation implies that there is a cooperative interaction between transition dipoles of increased density that favors light emission but infavors charge dissociation. This provides a critical understanding on why OIHPs can function as efficient photovoltaic and light-emitting materials at low and high excitation intensity, respectively. As has been widely reported that orientation of the transition dipole moments of an excited state is an critical factor influencing the performance in organic optoelectronic devices [33,34] and densitydependent excited-state behaviors are also significant topics in both photovoltaic and light-emitting devices. However, the polarization effects on optoelectronic behaviors in device-operating condition has never been clarified in OIHP devices. Our observations support the existence of polarized transition dipoles and their orientation-dependent impacts on photoluminescence and photocurrent in MAPbBr₃. Our work provides fundamental understandings in polarized excited states for further optimize performance of OIHP applications.

2. Experiment section

2.1. Device fabrication

The MAPbBr₃ perovskite precursor were prepared by dissolving lead bromide (PbBr₂, 99.98%, Alfa-Aesar), methylammonium bromide (MABr, 98%, Sigma-Aldrich) in a mixture solvent of N, N-dimethylmethanamide (DMF): dimethyl sulfoxide (DMSO) (7:3, v/v). The resulting solution was filtered using a polytetrafluoroethylene syringe filter (0.2 µm) before deposition. The devices in this work were fabricated with a structure of ITO/TiO_x/PEI/MAPbBr₃/PFO/MoO₃/Au. The TiO_x was deposited by spin-coating a diluted precursor (Titanium(IV) isopropoxide in isopropanol) onto the pre-cleaned ITO glass at 3000 rpm for 30 s followed by 450 °C annealing for 30 min in an oven in air condition. The PEI (polyethyleneimine solution, 50 wt% in H₂O, Sigma-Aldrich) was diluted in anhydride isopropanol with 0.02 wt% and spin-coated on top of the TiOx layer for surface modification at 5000 rpm for 60 s. Sequentially, the perovskite precursor solution was coated onto the substrate via a consecutive twostep spin-coating process at 1000 and 3000 rpm for 10 and 60 s, respectively. During the second spin step, 100 µL of toluene was deposited onto the substrate. The resulting films were then annealed at 90 °C for 5 min for better crystallization. After cooling to room temperature, PFO solution (10 mg ml⁻¹ in chlorobenzene) was spin-coated at 3000 rpm for 30 s as the hole transport layer. MoO₃ (10 nm) and Au electrodes (100 nm) were deposited using a thermal evaporation system through a mask under a high vacuum of less than 10^{-7} Torr. All devices were tested under ambient condition with encapsulation.

2.2. Photoluminescence measurements

The steady-state PL spectra were measured using Horiba Fluorolog system. The bias dependent PL was performed by illuminating the samples with 405-nm laser followed with optical lens and collected by a photodetector (Horiba). The 405-nm laser was followed by neutral filter 1, a polarizer and a half-wave plate. And the photodetector was placed behind a long-pass filter and neutral filter 2 in a position away from the reflected beam. The neutral filter 1 and 2 were used to adjust the photoexcitation intensity and protect the photodetector, respectively. The polarizer is used to ensure the excitation beam linearly polarized and the 495-nm long-pass filter (Thorlabs) is used to filter the 405-nm excitation beam so that the detected signal contains only 537-nm PL. By rotating the half-wave plate, the incident light could be switched between p- and s- polarized, where s-polarization was perpendicular to the incident plane and p-polarization was parallel to and in the incident plane. Notably the PL spectrometer was not an option in polarization dependent photoluminescence measurement because the gratings in the spectrometer was also polarization dependent. The PL lifetimes of transition dipoles under p- and s- photoexcitations were measured by using the time correlated single photon counting (TCSPC) system and anisotropy mode integrated in Horiba Fluorolog system with the 405 nm nanoLED excitation.

3. Results and discussion

The experiment setup is shown in Fig. 1. The built-in field comes from the difference in the work functions between two electrodes, pointing from ITO to MoO_3/Au . A 405-nm laser is used as the linearly polarized photoexcitation, of which the polarization orientation can be switched between p and s. The p-polarized light, as shown in Fig. 1a, with the polarization parallel to the incidence plane YZ, will generate p-polarized transition dipoles with the orientation approximately parallel to the built-in field (V_{bi}), while the s-polarized light, with the

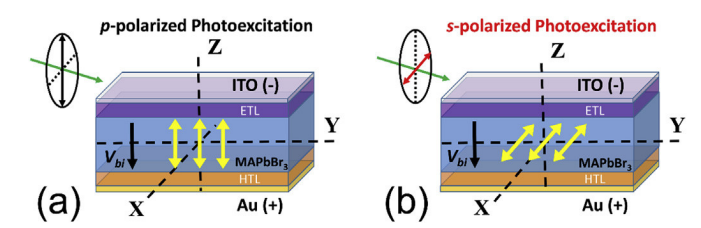


Fig. 1. Geometry for (a) *p*- and (b) *s*-polarized photoexcitation. The green arrow shows the incident light. The double-end arrows on the incident light show the polarization of photoexcitation, (a) the black for *p*- polarization and (b) the red for *s*- polarization respectively. The yellow double-end arrows in the devices show the orientation of photo-induced polarized transition dipoles.

polarization perpendicular to the incidence plane YZ, will generate s-polarized transition dipoles with the orientation perpendicular to the built-in field (V_{bi}) (Fig. 1b). To explore the response of p- and s- transition dipoles, such as charge dissociation, radiative recombination and polarization relaxation, under device-operating condition, the PL intensity and photocurrent density as a function of external bias were measured in the OIHP devices with the architecture of ITO/TiO $_x$ /PEI/MAPbBr $_3$ /PFO/MoO $_3$ /Au. The direction of the external bias is the same as the built-in field, so the total electric field in the device will be enhanced. In order to exclude the reflection difference between p- and s-polarized oblique incidence, the actual photoexcitation intensity which transmitted to the perovskite layer was calculated in the multilayered device based on Fresnel Equation [35,36].

To investigate the radiative recombination and dissociation of p-and s- polarized transition dipoles, PL intensity of the MAPbBr $_3$ layer was monitored as a function of applied bias under p- and s- polarized photoexcitation. Here, to study the field-induced PL quenching, the reduction of the PL intensity, namely Φ_{PL} , under bias — V was defined as

$$\Phi_{PL}(V) = \frac{I_{PL}(0) - I_{PL}(V)}{I_{PL}(0)} \times 100\%$$
(1)

where $I_{PL}(V)$ is the PL intensity under negative bias -V (V > 0) and $I_{PL}(0)$ is the PL intensity under zero bias, or short-circuit condition of the device. As can be seen in Fig. 2a, $\Phi_{PL}(V)$ increases when the absolute value of negative bias increases. It is known that negative bias will suppress the PL intensity due to the field-enhanced charge dissociation, therefore the slope $(\partial \Phi_{PL}/\partial V)$ of non-saturated region indicate the relative magnitude of field-induced charge dissociation [37,38]. An external bias ranged from -1 to 0 V was applied to the device while the PL change percentage was monitored, as shown in Fig. 2a. The slopes of the $\Phi_{PL} - V$ curves were calculated by linear fitting. Under $100 \,\mathrm{mW \, cm^{-2}}$ photoexcitation, the *p*-polarized excitation leads to a larger slope (0.54) than the s-polarized one (0.40), while under $400 \,\mathrm{mW}\,\mathrm{cm}^{-2}$ photoexcitation, the difference between p- and sslopes became much smaller. Before further discussion, it should be noted that the photoexcitation intensities mentioned here are the total incident power, the actual transmitted power is required to compare pand s- slopes under the same excitation intensity. The transmission of multilayered devices can be calculated by using the Fresnel Equation. For MAPbBr₃, with refractive index $n \approx 2.2$ [39], the calculation predicts a transmission of 75.96% and 50.60% for p- and s- polarized light, respectively, when the incident angle is 80°. As a result, in the case of 100, 200, 400 and 800 mW cm⁻² incident laser intensity, the actual photoexcitation intensities are 75.96, 151.92, $607.68 \,\mathrm{mW \, cm^{-2}}$ for the *p*-polarized excitation, and 50.60, 101.20, 202.40, 404.80 mW cm⁻² for the s-polarized excitation. Consequently, the p- and s- slopes as a function of actual photoexcitation intensity are shown in Fig. 2b. Two phenomena are observed.

Firstly, we observe that the transition dipoles generated by the p-and s- polarized photoexcitation show distinct field-induced dissociation rates. The p-polarized transition dipoles always encountered a

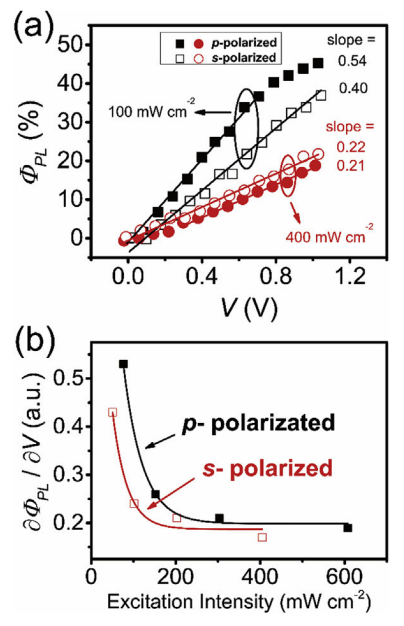


Fig. 2. (a) PL reduction Φ_{PL} as a function of V, where V > 0 is the absolute value of the negative bias -V, under 100 mW cm⁻² and 400 mW cm⁻² photoexcitation intensity using 405-nm laser as the polarized photoexcitation. The dots are experimental data, and solid lines and corresponding slopes are linear fitting results. (b) The slopes $(\partial \Phi_{PL}/\partial V)$ as a function of excitation intensity for p- and s- polarized photoexcitation. The dots are $\Phi_{PL} - V$ slopes extracted from measured data under different excitation intensities, and the solid lines are guide lines.

larger field-induced dissociation compared to s-polarized transition dipoles under the same excitation intensities. Based on the orientation of p- and s- polarized transition dipoles as shown in Fig. 1, It can be concluded that the polarization orientation plays a significant role in field-induced charge dissociation, which is an evidence that polarized transition dipoles, or photo-induced polarization, exist in polycrystal-line MAPbBr₃ films during the development of PL. Important issues, such as physical origins of polarization memories or polarization loss during electron relaxation, will be clarified later.

Secondly, a decrease on field-induced PL quenching can be observed for both *p*- and *s*- polarized transition dipoles with increasing excitation intensity, which has also been observed in our previous study [40]. It provides the evidence that the field-induced charge dissociation is highly dependent on the density of excited states in OIHPs. At higher density, the cooperative interaction between transition dipoles leads to an enhanced dipole-dipole interaction, which favors light emission and infavors charge dissociation, according to Fig. 2b. Therefore, both *p*-and *s*- polarized transition dipoles show decreasing field-driven dissociation under high excitation intensity. The decreasing field-induced charge dissociation rate suggests the existence of cooperative interaction between excited states to suppress charge dissociation at high excitation density, which can be supported by the high PL quantum efficiency observed in solid-state perovskites [41,42].

To verify the field-induced dissociation of p- and s- polarized transition dipoles, the photocurrent was probed along with PL. As shown in Fig. 3a, it can be observed that the dark current (grey line), or injected current, is close to zero under bias range between 0 and $-2\,\mathrm{V}$, so the total current J can be considered equal to the photocurrent in further discussion. To clearly show the charge dissociation of polarized transition dipoles under electric field, the change of photocurrent as a function of negative bias is shown in Fig. 3b. Photocurrent change $\Phi_J(V)$ under bias -V is defined as

$$\Phi_J(V) = \frac{J(V) - J(0)}{J(0)} \times 100\%$$
 (2)

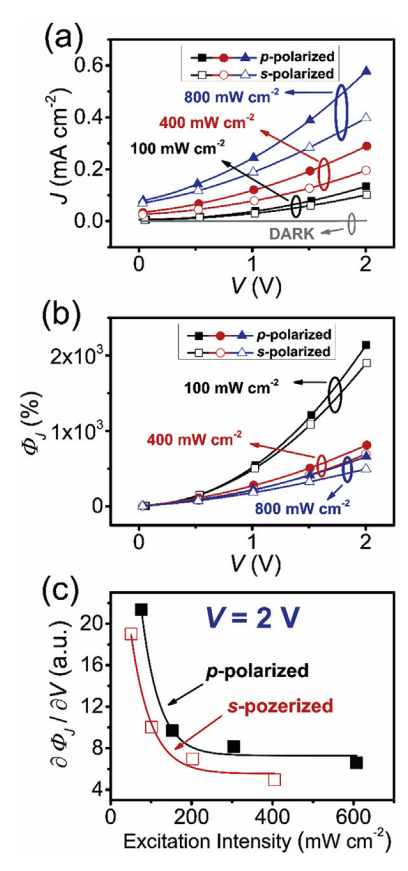


Fig. 3. (a) Photocurrent (J) and (b) photocurrent change (Φ_I) as a function of V (V > 0 is the value of the negative bias -V). (c) The slopes ($\partial \Phi_I/\partial V$) as a function of excitation intensity for p- and s- polarized photoexcitation, in which the dots are $\Phi_I - V$ slopes at 2 V negative bias under distinct excitation intensities and the solid lines are guide lines.

where J(V) is the photocurrent density under bias -V(V>0) and J(0) is the short-circuit current density. It can be seen that the p-polarized excitation always exhibits a higher Φ_I than the s-polarized excitation with the same intensity. The slopes of $\Phi_I - V$ curves, or $\partial \Phi_I/\partial V$, reflects the field-induced charge dissociation. To verify the field-induced charge dissociation behavior under the same actual excitation intensity, the slopes versus the actual excitation intensity under a negative bias of 2V is shown in Fig. 3c. Clearly, Fig. 3c shows consistent results with Fig. 2b that p-slopes are larger than s-slopes, implying that the quenched emissive excited states dissociates into free charge carriers which gives rise to the photocurrent. When excitation intensity increases, the magnitude of field-induced photocurrent enhancement is decreased, implying the decreased field-induced dissociation rate due to the cooperative interaction at increased density of transition dipoles.

The PL lifetimes were also measured under device-operating condition for p- and s- polarized excitations, respectively, to show their distinct field-induced radiative recombination of transition dipoles. The average PL lifetimes, $\langle \tau \rangle$, of p- and s- transition dipoles are calculated and summarized in Table S1 in supporting information. To explicitly demonstrate the field-induced decay, we present the PL intensity difference when the negative bias changes from 0 to 1 V. The PL intensity change ΔI is defined as $\Delta I = (I_{V=1} - I_{V=0})/I_{V=0}$, where $I_{V=1}$ and $I_{V=0}$ are the PL intensities when the negative bias is 1 V and 0 V, respectively, as shown in Fig. 4. It is observed that PL lifetime of p-polarized dipoles shows a much larger field-induced decay than s-polarized dipoles, which indicates that the dissociation of p-polarized dipoles are more responsive to the electric field than the s-polarized dipoles. Before further discussion, it is critical to be aware of the timescales of exciton dissociation, polarization relaxation and radiative. The timescale of

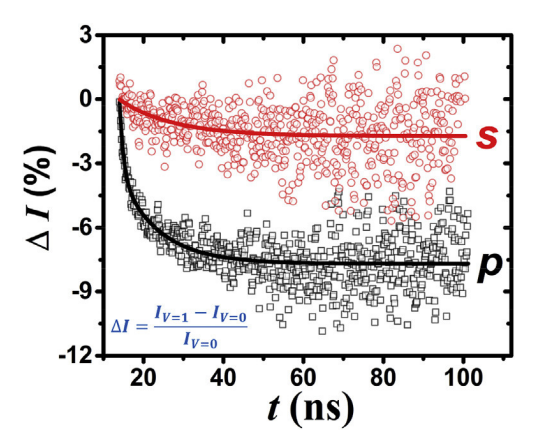


Fig. 4. PL decays of p- (black) and s- (red) polarized transition dipoles in MAPbBr₃ devices were measured under 0 V and -1 V. The intensity difference (ΔI) of PL is defined as $\Delta I = (I_{V=-1} - I_{V=0})/I_{V=0}$, where $I_{V=-1}$ and $I_{V=0}$ are the PL intensities under -1 V and 0 V, respectively.

polarization relaxation in OIHP thin film ranges from several to 150 ps at room temperature [17,18,32]. Besides, it has been reported in MAPbBr₃ that exciton dissociation is in sub-picosecond timescale [43], and radiative combination is in nanoseconds [44]. In this study, the PL lifetime of MAPbBr3 is measured to be 106 ns and 36 ns in bulk perovskite films and in devices, respectively, using time-resolved PL measurement (see Fig. S1 and Table S1, in the Supporting Information). Therefore, the polarization relaxation is considered to happen faster than radiative recombination and slower than exciton dissociation. Consequently, p- and s- polarized transition dipoles encounter different dissociation rates, which leads to different PL emission. On the other hand, photo-induced polarization, due to its picosecond-timescale relaxation, is in electronic polarization regime with a frequency of 10¹⁵ Hz. We can see that photo-induced electronic polarization is consequently converted to dielectric polarization at dipolar polarization regime in device-operating condition, which has much more significant impact on device performance. The conclusion was proved by the observation that p- and s- transition dipoles lead to distinct PL and photocurrent outputs. Structure asymmetry in OIHP films provides the origins for this conversion. Interestingly, we did not observe a polarized emission in steady-state PL measurement. This means that the transition dipoles have become randomized when radiative recombination occurs. Clearly, the PL lifetime measurements provide a deeper insight that transition dipoles are the microscopic origins of polarization ef-

The orientation effect of transition dipoles is of great significance and broad implications for improving the performance of perovskite applications such as solar cells and LEDs. It has been reported theoretically and experimentally that horizontally polarized transition dipoles results in higher outcoupling efficiency as compared to vertically polarized transition in thin-film LEDs [33,34]. For example, as the ratio of horizontal transition dipoles increases from 0.67 to 0.78, the EQE of Ir (ppy)₃ based OLEDs increases significantly from 26.3% to 32.3% [34]. To evaluate the ratio of vertical transition dipoles in MAPbBr₃ LEDs, we measured the edge emission of electroluminescence (EL) and observed a polarization degree of 0.22 (see Fig. S2, in the Supporting Information). It indicates that vertically polarized transition dipoles lead to significant energy loss in perovskite LEDs due to edge emission. Our results reveal that polarizing transition dipoles is promising to improve the performance of perovskite LEDs by reducing the ratio of vertical transition dipoles. The EQE can be improved by 50% if all transition dipoles are horizontally oriented instead of random orientation (see Note S1, in the Supporting Information). For the solar cells, on the contrast to LEDs, an alternative method to improve the efficiency is to increase the ratio of vertical transition dipoles, due to the larger field-

induced dissociation of *p*-polarized transition dipoles as shown in Fig. 3c. The efficiency of perovskite solar cells could be improved by 18.2% if all transition dipoles are vertically oriented instead of random orientation (see Note S2, in the Supporting Information). Therefore, the orientation of transition dipoles has a direct impact on the performance of IOHP applications. Many works have shown that the orientation of transition dipoles is associated with domain geometry in polycrystalline IOHP films which can be controlled by post treatments [31,45–47]. These works provide feasible methods to improve the device performance based on our results.

It is necessary to clarify two issues in observed phenomena before proposing the mechanism. Firstly, transient polarization memory, which originates from structural asymmetry, was observed in MAPbBr₃ despite of its symmetric cubic lattice. Secondly, polarization effects on PL and photocurrent was observed despite of the polarization loss due to above-bandgap photoexcitation. It is known that transient polarization memory is based on structural anisotropy in hybrid perovskites [17,18]. In polycrystalline MAPbBr₃ thin films, despite of intrinsic cubic lattice in nanoscale grains, the distortion of local crystal lattice, due to the defects at grain boundaries, contributes to structural asymmetry and could acts as the origin of transient polarization memory. Besides, the soft-disordered methylammonium sublattice if crystal grains also contributes to the structural asymmetry [48]. Rivett and coworkers reported in their recent work that there is strong coupling between local anharmonic lattice dynamics and optical properties of electronic states in these materials, which enables dynamic structural anisotropy and consequently leads to polarization anisotropy [32]. They showed polarization anisotropy in MAPbBr3 bulk films, which is confirmed by our observations. Their work also mentioned the polarization loss issue in lead halide perovskites when utilizing abovebandgap photoexcitation. In our work, a 405-nm laser (3.1 eV) was applied to excite MAPbBr3 with 2.3 eV bandgap. It is expected that the polarization memory can be hardly maintained in MAPbBr₃ films due to significant polarization loss when electrons relax from higher energy level to the bottom of the conduction band. However, it should be emphasized that in our study, the PL and photocurrent under p- and spolarized photoexcitation was measured under device-operating condition, which is significantly different from the bulk-film condition in the above work. Localized dynamic polarizations from charged defects and ions will interact with photo-induced polarization, and consequently accelerates the relaxation of polarization. Under the electric field in device-operating condition, localized dynamic polarization can be partially frozen and consequently reduce the polarization loss. These results are very significant for further designing perovskite-based photovoltaic and light-emitting applications.

We propose that vertically *p*- and horizontally *s*- polarized transition dipoles experience distinct field-induced dissociation rates under the influence of electrical field at device-operating condition. However, when photoexcitation intensity increases, the established cooperative interaction between transition dipoles can decrease the field-induced dissociation rates for both p- and s- polarized transition dipoles (as shown in Figs. 2b and 3c). As shown in Fig. 5, when the p- and s- polarized photoexcitation is applied, the p- and s- polarized transition dipoles are generated correspondingly. Compared to s-polarized transition dipoles, the p-polarized transition dipoles encounter larger fieldinduced dissociation due to the orientation parallel to the electric field, leading to larger field-induced PL quenching and larger photocurrent enhancement. The experimental observations provide the evidence that photo-induced polarization does exist during the development of PL and photocurrent. Noted that polarized transition dipoles experience three dominative processes in this phenomenon: (1) charge dissociation, (2) radiative recombination and (3) polarization relaxation. As we presented in this study, the timescales of charge dissociation, polarization relaxation and radiative recombination are sub-picoseconds [43], several to 150 ps [17,18,32], and 106 ns (see Fig. S1, in the Supporting Information), respectively. The increased density of

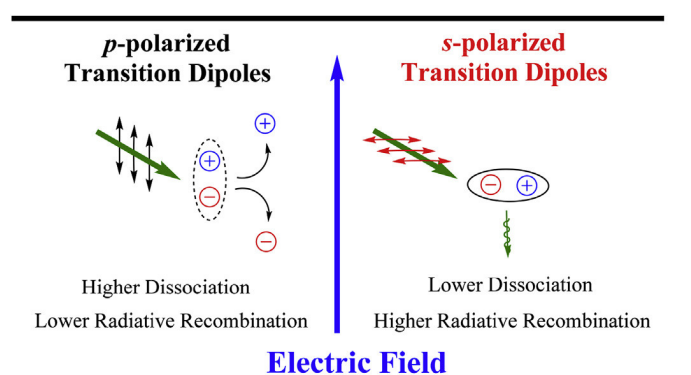


Fig. 5. Field-induced dissociation and radiative recombination of p- and s-polarized transition dipoles in electric field.

transition dipoles under higher excitation intensities enhances the dipole-dipole interaction. The enhanced cooperative interaction decreases the field-induced dissociation rates, or increases the dissociation time equivalently, leading to decreased PL quenching and decreased photocurrent enhancement under higher excitation intensity. This provides a critical understanding on why organic-inorganic hybrid perovskites can function as efficient photovoltaic and light-emitting materials at low and high excitation intensity, respectively.

4. Conclusions

In this work, we presented that in the perovskite (MAPbBr₃) devices the photo-induced horizontally and vertically polarized transition dipoles experience distinct field-induced dissociation rates under deviceoperating condition. The vertically p-polarized transition dipoles, with orientation parallel to the electric field, lead to a larger field-induced PL quenching compared to horizontally s-polarized transition dipoles, with orientation perpendicular to the electric field. This experimental observation indicates that photo-induced polarization can indeed exist during the development of photocurrent and PL in OIHP devices. It also proved that the photo-induced electronic polarization at high-frequency regime can be converted to photoinduced dielectric polarization at dipolar polarization regime and consequently influences the device performance. Structural asymmetry in the bulk film provides the necessary condition to realize from photoinduced electronic polarization to photoinduced dielectric polarization at dipolar polarization regime. When increasing photoexcitation intensity, the cooperative interaction between transition dipoles can decrease their field-driven dissociation rates, leading to reduced PL quenching and photocurrent enhancement in OIHP devices. This work provides not only critical understandings on why OIHPs can function as efficient photovoltaic and light-emitting materials at low and high excitation intensities, respectively, but also experimental guidelines for further optimization of OIHP optoelectronic applications.

Acknowledgement

This research was supported by the financial supports from Air Force Office of Scientific Research (AFOSR) under the grant number FA 9550-15-1-0064, AOARD (FA2386-15-1-4104) and National Science Foundation (NSF-1911659).

Appendix A. Supplementary data

Supplementary data to this article can be found online at https://doi.org/10.1016/j.nanoen.2019.104004.

References

- [1] H.J. Snaith, Perovskites: the emergence of a new era for low-cost, high-efficiency solar cells, J. Phys. Chem. Lett. 4 (2013) 3623–3630.
- [2] A. Kojima, K. Teshima, Y. Shirai, T. Miyasaka, Organometal halide perovskites as visible-light sensitizers for photovoltaic cells, J. Am. Chem. Soc. 131 (2009) 6050–6051.
- [3] M.A. Green, Y. Hishikawa, E.D. Dunlop, D.H. Levi, J. Hohl-Ebinger, M. Yoshita, A.W.Y. Ho-Baillie, Solar cell efficiency tables (Version 53), Prog. Photovolt. Res. Appl. (2019), https://doi.org/10.1002/pip.3102.
- [4] W.S. Yang, B.-W. Park, E.H. Jung, N.J. Jeon, Y.C. Kim, D.U. Lee, S.S. Shin, J. Seo, E.K. Kim, J.H. Noh, Iodide management in formamidinium-lead-halide-based perovskite layers for efficient solar cells, Science 356 (2017) 1376–1379.
- [5] M. Ahmadi, T. Wu, B. Hu, A review on organic-inorganic halide perovskite photodetectors: device engineering and fundamental physics, Adv. Mater. 29 (2017) 1605242, https://doi.org/10.1002/adma.201605242.
- [6] L. Meng, E. Yao, Z. Hong, H. Chen, P. Sun, Z. Yang, G. Li, Y. Yang, Pure for-mamidinium-based perovskite light-emitting diodes with high efficiency and low driving voltage, Adv. Mater. 29 (2017) 1603826.
- [7] Z. Xiao, R.A. Kerner, L. Zhao, N.L. Tran, K.M. Lee, T.-W. Koh, G.D. Scholes, B.P. Rand, Efficient perovskite light-emitting diodes featuring nanometre-sized crystallites, Nat. Photonics 11 (2017) 108.
- [8] H. Seo, H. Kim, J. Lee, M. Park, S. Jeong, Y. Kim, S. Kwon, T. Han, S. Yoo, T. Lee, Efficient flexible organic/inorganic hybrid perovskite light-emitting diodes based on graphene anode, Adv. Mater. 29 (2017) 1605587.
- [9] B.R. Sutherland, E.H. Sargent, Perovskite photonic sources, Nat. Photonics 10 (2016) 295–302.
- [10] Y. Jia, R.A. Kerner, A.J. Grede, B.P. Rand, N.C. Giebink, Continuous-wave lasing in an organic-inorganic lead halide perovskite semiconductor, Nat. Photonics 11 (2017) 784–788.
- [11] S.A. Veldhuis, P.P. Boix, N. Yantara, M. Li, T.C. Sum, N. Mathews, S.G. Mhaisalkar, Perovskite materials for light-emitting diodes and lasers, Adv. Mater. 28 (2016) 6804–6834, https://doi.org/10.1002/adma.201600669.
- [12] D. Li, H. Cheng, Y. Wang, Z. Zhao, G. Wang, H. Wu, Q. He, Y. Huang, X. Duan, The effect of thermal annealing on charge transport in organolead halide perovskite microplate field-effect transistors, Adv. Mater. 29 (2017) 1601959.
- [13] A. Yusoff, R. bin Mohd, H.P. Kim, X. Li, J. Kim, J. Jang, M.K. Nazeeruddin, Ambipolar triple cation perovskite field effect transistors and inverters, Adv. Mater. 29 (2017).
- [14] S.P. Senanayak, B. Yang, T.H. Thomas, N. Giesbrecht, W. Huang, E. Gann, B. Nair, K. Goedel, S. Guha, X. Moya, Understanding charge transport in lead iodide perovskite thin-film field-effect transistors, Sci. Adv. 3 (2017) e1601935.
- [15] Y. Kutes, L. Ye, Y. Zhou, S. Pang, B.D. Huey, N.P. Padture, Direct observation of ferroelectric domains in solution-processed CH3NH3PbI3 perovskite thin films, J. Phys. Chem. Lett. 5 (2014) 3335–3339.
- [16] Z. Xiao, Y. Yuan, Y. Shao, Q. Wang, Q. Dong, C. Bi, P. Sharma, A. Gruverman, J. Huang, Giant switchable photovoltaic effect in organometal trihalide perovskite devices, Nat. Mater. 14 (2015) 193.
- [17] Y. Zhai, C.X. Sheng, C. Zhang, Z.V. Vardeny, Ultrafast spectroscopy of photoexcitations in organometal trihalide perovskites, Adv. Funct. Mater. 26 (2016) 1617–1627.
- [18] C. Sheng, C. Zhang, Y. Zhai, K. Mielczarek, W. Wang, W. Ma, A. Zakhidov, Z.V. Vardeny, Exciton versus free carrier photogeneration in organometal trihalide perovskites probed by broadband ultrafast polarization memory dynamics, Phys. Rev. Lett. 114 (2015) 116601.
- [19] Y. Deng, Z. Xiao, J. Huang, Light-induced self-poling effect on organometal trihalide perovskite solar cells for increased device efficiency and stability, Adv. Energy Mater. 5 (2015) 1500721.
- [20] Q. Dong, J. Song, Y. Fang, Y. Shao, S. Ducharme, J. Huang, Lateral-structure single-crystal hybrid perovskite solar cells via piezoelectric poling, Adv. Mater. 28 (2016) 2816–2821.
- [21] L. Zhao, J. Gao, Y.L. Lin, Y. Yeh, K.M. Lee, N. Yao, Y. Loo, B.P. Rand, Electrical stress influences the efficiency of CH3NH3PbI3 perovskite light emitting devices, Adv. Mater. 29 (2017) 1605317.
- [22] L. Bertoluzzi, R.S. Sanchez, L. Liu, J.-W. Lee, E. Mas-Marza, H. Han, N.-G. Park, I. Mora-Sero, J. Bisquert, Cooperative kinetics of depolarization in CH3NH3Pbl3 perovskite solar cells, Energy Environ. Sci. 8 (2015) 910–915.
- [23] H.-S. Kim, S.K. Kim, B.J. Kim, K.-S. Shin, M.K. Gupta, H.S. Jung, S.-W. Kim, N.-G. Park, Ferroelectric polarization in CH3NH3PbI3 perovskite, J. Phys. Chem. Lett. 6 (2015) 1729–1735.
- [24] S. Meloni, T. Moehl, W. Tress, M. Franckevičius, M. Saliba, Y.H. Lee, P. Gao, M.K. Nazeeruddin, S.M. Zakeeruddin, U. Rothlisberger, Ionic polarization-induced current-voltage hysteresis in CH3NH3PbX3 perovskite solar cells, Nat. Commun. 7 (2016) 10334.
- [25] Y. Kitanaka, K. Hirano, M. Ogino, Y. Noguchi, M. Miyayama, C. Moriyoshi, Y. Kuroiwa, Polarization twist in perovskite ferrielectrics, Sci. Rep. 6 (2016) 32216.
- [26] K. Miyata, D. Meggiolaro, M.T. Trinh, P.P. Joshi, E. Mosconi, S.C. Jones, F. De Angelis, X.-Y. Zhu, Large polarons in lead halide perovskites, Sci. Adv. 3 (2017) e1701217.
- [27] S.A. Bretschneider, I. Ivanov, H.I. Wang, K. Miyata, X. Zhu, M. Bonn, Quantifying polaron formation and charge carrier cooling in lead-iodide perovskites, Adv. Mater. (2018) 1707312.
- [28] S.M. Young, A.M. Rappe, First principles calculation of the shift current photovoltaic effect in ferroelectrics, Phys. Rev. Lett. 109 (2012) 116601.
- [29] V.M. Fridkin, Bulk photovoltaic effect in noncentrosymmetric crystals, Crystallogr.

- Rep. 46 (2001) 654-658.
- [30] T. Choi, S. Lee, Y.J. Choi, V. Kiryukhin, S.-W. Cheong, Switchable ferroelectric diode and photovoltaic effect in BiFeO3, Science 324 (2009) 63–66.
- [31] B.R. Watson, B. Yang, K. Xiao, Y.-Z. Ma, B. Doughty, T.R. Calhoun, Elucidation of perovskite film micro-orientations using two-photon total internal reflectance fluorescence microscopy, J. Phys. Chem. Lett. 6 (2015) 3283–3288.
- [32] J.P.H. Rivett, L.Z. Tan, M.B. Price, S.A. Bourelle, N.J.L.K. Davis, J. Xiao, Y. Zou, R. Middleton, B. Sun, A.M. Rappe, Long-lived polarization memory in the electronic states of lead-halide perovskites from local structural dynamics, Nat. Commun. 9 (2018) 3531.
- [33] J.-S. Kim, P.K.H. Ho, N.C. Greenham, R.H. Friend, Electroluminescence emission pattern of organic light-emitting diodes: implications for device efficiency calculations, J. Appl. Phys. 88 (2000) 1073–1081.
- [34] K. Kim, C. Moon, J. Lee, S. Kim, J. Kim, Highly efficient organic light-emitting diodes with phosphorescent emitters having high quantum yield and horizontal orientation of transition dipole moments, Adv. Mater. 26 (2014) 3844–3847.
- [35] E. Hecht, Optics, Addison-Wesley, 1987.
- [36] M.B. Price, J. Butkus, T.C. Jellicoe, A. Sadhanala, A. Briane, J.E. Halpert, K. Broch, J.M. Hodgkiss, R.H. Friend, F. Deschler, Hot-carrier cooling and photoinduced refractive index changes in organic-inorganic lead halide perovskites, Nat. Commun. 6 (2015) 8420.
- [37] J. Szmytkowski, W. Stampor, J. Kalinowski, Z.H. Kafafi, Electric field-assisted dissociation of singlet excitons in tris-(8-hydroxyquinolinato) aluminum (III), Appl. Phys. Lett. 80 (2002) 1465–1467.
- [38] D. Veldman, O. Ipek, S.C.J. Meskers, J. Sweelssen, M.M. Koetse, S.C. Veenstra, J.M. Kroon, S.S. van Bavel, J. Loos, R.A.J. Janssen, Compositional and electric field dependence of the dissociation of charge transfer excitons in alternating polyfluorene copolymer/fullerene blends, J. Am. Chem. Soc. 130 (2008) 7721–7735.
- [39] P.F. Ndione, Z. Li, K. Zhu, Effects of alloying on the optical properties of organic-inorganic lead halide perovskite thin films, J. Mater. Chem. C. 4 (2016) 7775–7782.
- [40] Y. Hsiao, T. Wu, M. Li, B. Hu, Magneto-optical studies on spin-dependent charge recombination and dissociation in perovskite solar cells, Adv. Mater. 27 (2015) 2899–2906.
- [41] F. Deschler, M. Price, S. Pathak, L.E. Klintberg, D.-D. Jarausch, R. Higler, S. Hüttner, T. Leijtens, S.D. Stranks, H.J. Snaith, High photoluminescence efficiency and optically pumped lasing in solution-processed mixed halide perovskite semiconductors, J. Phys. Chem. Lett. 5 (2014) 1421–1426.
- [42] S.D. Stranks, V.M. Burlakov, T. Leijtens, J.M. Ball, A. Goriely, H.J. Snaith, Recombination kinetics in organic-inorganic perovskites: excitons, free charge, and subgap states, Phys. Rev. Appl. 2 (2014) 34007.
- [43] C.S. Ponseca Jr., T.J. Savenije, M. Abdellah, K. Zheng, A. Yartsev, T. Pascher, T. Harlang, P. Chabera, T. Pullerits, A. Stepanov, Organometal halide perovskite solar cell materials rationalized: ultrafast charge generation, high and microsecondlong balanced mobilities, and slow recombination, J. Am. Chem. Soc. 136 (2014) 5189–5192.
- [44] H. Cho, S.-H. Jeong, M.-H. Park, Y.-H. Kim, C. Wolf, C.-L. Lee, J.H. Heo, A. Sadhanala, N. Myoung, S. Yoo, Overcoming the electroluminescence efficiency limitations of perovskite light-emitting diodes, Science 350 (2015) 1222–1225.
- [45] P. Fassl, S. Ternes, V. Lami, Y. Zakharko, D. Heimfarth, P.E. Hopkinson, F. Paulus, A.D. Taylor, J. Zaumseil, Y. Vaynzof, Effect of crystal grain orientation on the rate of ionic transport in perovskite polycrystalline thin films, ACS Appl. Mater. Interfaces 11 (2018) 2490–2499.
- [46] T. Zhao, H. Liu, M.E. Ziffer, A. Rajagopal, L. Zuo, D.S. Ginger, X. Li, A.K.Y. Jen, Realization of a highly oriented MAPbBr3 perovskite thin film via ion exchange for ultrahigh color purity green light emission, ACS Energy Lett. 3 (2018) 1662–1669.
- [47] N. Giesbrecht, J. Schlipf, L. Oesinghaus, A. Binek, T. Bein, P. Müller-Buschbaum, P. Docampo, Synthesis of perfectly oriented and micrometer-sized MAPbBr3 perovskite crystals for thin-film photovoltaic applications, ACS Energy Lett. 1 (2016) 150–154.
- [48] P.E. Evans, M. Pink, A.A. Zhumekenov, G. Hao, Y. Losovyj, O.M. Bakr, P.A. Dowben, A.J. Yost, Rotationally free and rigid sublattices of the single crystal perovskite CH3NH3PbBr3 (001): the case of the lattice polar liquid, J. Phys. Chem. C 122 (2018) 25506–25514.



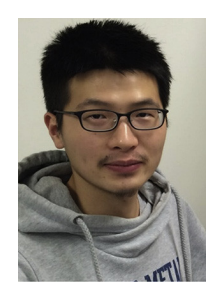
Dr. Shengbo Ma is a research associate in Joint Institute for Advanced Materials (JIAM), Department of Materials Science, the University of Tennessee, Knoxville. He received his B. S. degree in physics and Ph. D degree in optics in Peking University, China. His current research is focused on the behaviors of excited states in the light-emitting diodes based on organic-inorganic hybrid perovskites.



Hengxing Xu is currently pursuing his Ph.D under the supervision of Prof. Bin Hu in the Department of Material Science and Engineering at the University of Tennessee, Knoxville. He received his B.S. degree in materials science and engineering at Beijing Institute of Technology, China, and M.S. degree in condensed matter physics at Beijing University of Aeronautics & Astronautics, China. His current research interests focus on spin related optoelectronic properties in organic-inorganic hybrid perovskites.



Ting Wu is currently pursuing her Ph.D. under the supervision of Prof. Bin Hu in the Department of Material Science and Engineering at the University of Tennessee, Knoxville, USA. She received her B.S. in polymer science (2009) and M.S. in materials science (2012) at Sichuan University, China. Her current research interests focus on materials development, device engineering and fundamental physics in perovskite solar cells.



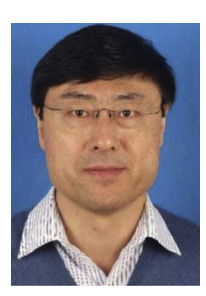
Miaosheng Wang is currently pursuing his Ph.D. degree in the Department of Materials Science and Engineering at the University of Tennessee, Knoxville, USA. He received the B.S. degree in Materials Physics (2015) in School of Physics and Technology at Wuhan University, China. His current research interests focus on optoelectronics, spintronics, ultrafast laser spectroscopy and the underlying fundamental physics in organic & hybrid perovskites materials.



Dr. Ping Chen is an associate professor in School of Physical Science and Technology, Southwest University, China. He received his Ph. D from Jilin University, China, in 2014. He is currently working as a visiting postdoc in Department of Materials Science and Engineering, University of Tennessee, Knoxville, USA. His research focuses on materials development, device engineering and fundamental physics in organic-inorganic hybrid perovskite light-emitting diodes.



Dr. Jiajun Qin is currently working as a visiting researcher at Department of Physics, Chemistry and Biology, Linköping University, Sweden. He received his Ph.D. from Fudan University, Shanghai, China in 2019. His research interests have included device physics of organic/perovskite memory, light emitting and solar cells. Specially, his current research focuses on investigating the working mechanisms as well as developing electrically pumped lasers.



Professor Bin Hu received his Ph. D from the Chinese Academy of Sciences in Condensed Matter Physics. He then worked as a postdoc at the Institute of Molecular Spectroscopy – CNR, Bologna, Italy with Professor Carlo Taliani, and as research scientist at the University of Massachusetts/Amherst with Professor Frank Karasz. In 2002, he joined the faculty in the Department of Materials Science and Engineering at the University of Tennessee, Knoxville. His research includes spin-dependent processe in excited states, magneto-optic studies on photovoltaic and thermoelectric processes at different length scales, and lasing actions in ferroelectrically semiconducting materials.